第 35 卷第 6 期 无 机 化 学 学 报 Vol.35 No.6
2019 年 6 月 CHINESE JOURNAL OF INORGANIC CHEMISTRY 1109-1120

Salamo 型三核镍(Ⅱ)配合物的合成、晶体结构与 Hirshfeld 表面分析

于 盟 穆浩冉 刘玲芝 李 娜 白 杨 董秀延*
(兰州交通大学化学与生物工程学院,兰州 730070)

摘要: 合成了 2 种新设计的 Salamo 型配合物,{[Ni(L^1)(*n*-propanol)]$_2$(OAc)$_2$Ni}·2(*n*-propanol) (**1**)和{[Ni(L^2)(*n*-butanol)]$_2$(OAc)$_2$Ni}·2(*n*-butanol) (**2**),并用元素分析、红外光谱、紫外-可见光谱、Hirshfeld 表面分析和单晶 X 射线晶体学对其进行了表征。X 射线晶体学分析表明,配合物 **1** 和 **2** 均为对称的三核镍(Ⅱ)配合物。**1** 和 **2** 中的镍(Ⅱ)都是六配位的,形成了扭曲的八面体几何构型。晶体结构分析和 Hirshfeld 表面分析均表明,**1** 和 **2** 通过分子间氢键作用分别形成稳定的一维链状和二维超分子结构。

关键词: Salamo 型配体; 配合物; 合成; 晶体结构; Hirshfeld 表面分析
中图分类号: O614.81$^+$3 **文献标识码**: A **文章编号**: 1001-4861(2019)06-1109-12
DOI:10.11862/CJIC.2019.128

Syntheses, Structures and Hirshfeld Analyses of Trinuclear Ni(Ⅱ) Salamo-Type Complexes

YU Meng MU Hao-Ran LIU Ling-Zhi LI Na BAI Yang DONG Xiu-Yan*
(*School of Chemical and Biological Engineering, Lanzhou Jiaotong University, Lanzhou* 730070, *China*)

Abstract: Two newly designed complexes, {[Ni (L^1) (*n*-propanol)]$_2$ (OAc)$_2$Ni} ·2 (*n*-propanol) (**1**) and {[Ni (L^2) (*n*-butanol)]$_2$(OAc)$_2$Ni}·2(*n*-butanol) (**2**) derived from tetradentate Salamo-type chelating ligands (H_2L^1=5-methoxy-2,2′-(ethylenedioxybis(azomethine))diphenol and H_2L^2=4,4′-dinitro-2,2′-(ethylenediyldioxybis(nitrilomethylidyne)) diphenol) have been synthesized and characterized by elemental analyses, IR and UV-Vis spectra, Hirshfeld surfaces analyses and single crystal X-ray crystallography. X-ray crystallographic analyses showed that complexes **1** and **2** are all symmetric trinuclear Ni(Ⅱ) complexes. Nickel(Ⅱ) in both **1** and **2** is hexa-coordinated, forming a twisted octahedral geometry. Both crystal structure and Hirshfeld surface analysis indicate that **1** and **2** form stable one-dimensional chain and two-dimensional supramolecular structures, respectively, by intermolecular hydrogen bonding. CCDC: 1589650, **1**; 1589813, **2**.

Keywords: Salamo-type ligand; complex; synthesis; crystal structure; Hirshfeld analysis

0 Introduction

As we known, Salen and its derivatives[1-4] are extremely important N_2O_2 chelating ligands in organometallic and coordination chemistry. Not only their transition metal complexes[5-9] are widely studied in the biological fields[10-17], but also there are certain advantages in luminescent[18-25] and magnetic[26-31] materials, electrochemical fields[32-33], supramolecular constructions[34-38], and so on.

As derivatives of Salen, in recent years, our research mostly concentrated on the syntheses of Salamo-type ligands[39-46]. These compounds have been investigated in forming metal complexes with

收稿日期:2019-02-03。收修改稿日期:2019-03-28。
国家自然科学基金(No.21761018)和兰州交通大学优秀科研团队计划(No.201706)资助项目。
*通信联系人。E-mail:dxy568@163.com

interesting properties[47-48], and some works have been devoted to synthesize and characterize mono-[49], di- and multi-nuclear metal(Ⅱ) complexes bearing Salamo ligand and its derivatives[50-51]. Herein, as part of our ongoing interest in Salamo-type complexes, we have described the syntheses, crystal structures, and Hirshfeld surfaces analyses of two trinuclear Ni(Ⅱ) complexes, which were constructed from Salamo-type bisoxime ligands 5-methoxy-2,2′-(ethylenedioxybis(azomethine)) diphenol (H_2L^1) and 4,4′-dinitro-2,2′-(ethylenediyldioxybis(nitrilomethylidyne))diphenol (H_2L^2).

1 Experimental

1.1 Materials and methods

All chemical reagents are analytical pure reagents, which have not been purified before used. C, H and N analyses were obtained using a GmbH Vario EL V3.00 automatic elemental analyzer. Elemental analysis for Ni(Ⅱ) was conducted using an IRIS ER/S·WP-1 ICP atomic emission spectrometer. ^{1}H NMR spectra were recorded using a Bruker AVANCE DRX-400 spectrometer. The melting points were determined by microscopic melting point instrument made in Beijing Tektronix Instruments Limited Company. IR spectra were recorded on a VERTEX70 FT-IR spectrophotometer, with samples prepared as KBr (500~4 000 cm^{-1}) and CsI (100~500 cm^{-1}) pellets. UV-Vis absorption spectra were recorded on a Shimadzu UV-2550 spectrometer.

1.2 Synthesis of H_2L^1

The asymmetric Salamo-type ligand H_2L^1 was synthesized by a modified method reported in the earlier literature (Scheme 1)[24].

To an ethanol solution (30 mL) of 4-methoxy-2-hydroxybenzaldehyde (316.62 mg, 2.08 mmol) was added an ethanol solution (20 mL) of 1,2-bis(aminooxy) ethane (289.32 mg, 3.14 mmol). The mixture solution was heated at 50~55 ℃ for 5 h. The solution was concentrated in reduced pressure to obtain 210.37 mg of yellow solid, 2-(*O*-(1-ethyloxyamide))oxime-5-methophenol. Yield: 44.68%, m.p. 96~98 ℃. Anal. Calcd. for $C_{10}H_{14}N_2O_4$ (%): C 53.09, H 6.24, N 12.38; Found (%): C 53.08, H 6.25, N 12.36.

A solution of above-obtained 2-(*O*-(1-ethyloxyamide))oxime-5-methophenol (210.37 mg, 0.93 mmol) in ethanol (20 mL) was added dropwise to a solution of salicylaldehyde (107.03 mg, 0.88 mmol) in ethanol (15 mL), and the mixture was heated at 50~55 ℃ for 3 h. After cooling to room temperature, the solution was concentrated in reduced pressure. The residue was purified by column chromatography (SiO_2, chloroform/ethyl acetate, 10∶1, *V*/*V*) to afford 139.26 mg colorless flocculent crystalline solid (H_2L^1). Yield: 48.1%. m.p. 69~71 ℃. ^{1}H NMR (400 MHz, $CDCl_3$): δ 3.81 (s, 3H, CH_3), 4.44 (m, 4H, CH_2), 6.46~6.49 (m, 2H, ArH), 6.89~6.92 (d, *J*=12 Hz, 1H, ArH), 6.97~6.99 (d, *J*=8 Hz, 1H, ArH), 7.04~7.06 (d, *J*=8 Hz, 1H, ArH), 7.15~7.17 (d, *J*=8 Hz, 1H, ArH), 8.18 (s, 1H, CH=N), 8.24 (s, 1H, CH=N), 8.25 (s, 1H), 9.75 (s, 1H, OH), 9.92 (s, 1H, OH). Anal. Calcd. for $C_{17}H_{18}N_2O_5$(%): C 61.81, H 5.49, N 8.48; Found(%): C 61.80, H 5.50, N 8.49.

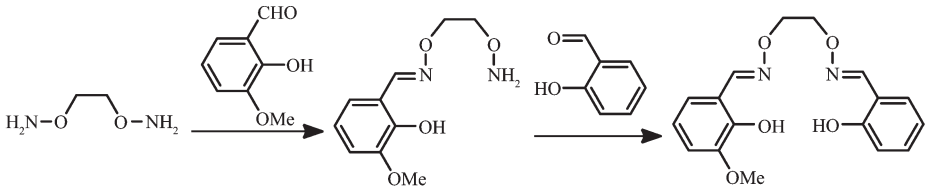

Scheme 1 Synthesis route of H_2L^1

1.3 Synthesis of H_2L^2

The reaction route is shown in Scheme 2. 4,4′-Dinitro-2,2′-(ethylenediyldioxybis (nitrilomethylidyne)) diphenol (H_2L^2) was synthesized according to the method reported earlier[39]. Yield: 80.0%, m.p. 202~203 ℃, Anal. Calcd. for $C_{16}H_{14}N_4O_8$(%): C 49.24, H 3.62, N 14.35. Found(%): C 49.33, H 3.58, N 14.04. ^{1}H NMR (400 MHz, DMSO-d_6): δ 4.44 (s, 4H), 7.03 (d, *J*=9.2 Hz, 2H), 8.09 (dd, *J*=9.2, 2.6 Hz, 2H), 8.35 (d, *J*=2.6 Hz, 2H), 8.37 (s, 2H), 10.13 (s, 2H, OH).

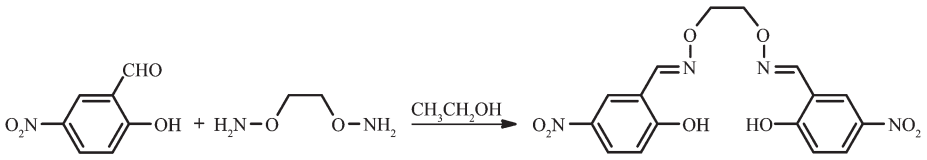

Scheme 2　Synthesis route of H_2L^2

1.4　Synthesis of complex 1

A *n*-propanol solution (3.0 mL) of nickel(Ⅱ) acetate tetrahydrate (2.46 mg, 0.01 mmol) was added to a dichloromethane solution (2.0 mL) of H_2L^1: 5-methoxy-2,2′-(ethylenedioxybis(azomethine))diphenol (3.31 mg, 0.01 mmol) at room temperature. After the mixture was stirred for 2 h, the mixture was filtered off. The resulting filtrate was left undisturbed for about one week to form block-like crystals suitable for X-ray crystallographic analysis. Yield: 40.5%. Anal. Calcd. for $C_{50}H_{70}Ni_3N_4O_{18}$(%): C 50.41, H 5.92, N 4.70; Ni 14.78; Found(%): C 50.60; H 5.98; N 4.52; Ni 14.62.

1.5　Synthesis of complex 2

A solution of nickel(Ⅱ) acetate tetrahydrate (2.48 mg, 0.01 mmol) in *n*-butanol (3 mL) was added dropwise to a solution of H_2L^2 (3.90 mg, 0.01 mmol) in acetonitrile (3 mL) at room temperature. The color of the mixing solution turned yellow immediately, and was stirring continually for 1h at room temperature. The mixture was filtered and the filtrate was allowed to stand at room temperature for about three weeks. The solvent was partially evaporated and several green prismatic single crystals suitable for X-ray crystallographic analysis were obtained. Yield: 47.8%. Anal. Calcd. for $C_{52}H_{70}Ni_3N_8O_{24}$(%): C 45.68, H 5.16, N 8.20, Ni 12.88; Found(%): C 45.90, H 5.22, N 8.02, Ni 12.63.

1.6　Crystal structure determinations of complexes 1 and 2

X-ray single crystal diffraction data of complexes **1** and **2** were recorded using a Super Nova Dual (Cu at zero) diffractometer with a monochromated Mo $K\alpha$ radiation (λ=0.710 73 nm) at 294.29(10) and 293.84(19) K, respectively. The Lp factor semi-empirical absorption corrections were applied using the SADABS program[52a]. The structures were solved by the direct methods (SHELXS-2014[52b]). All hydrogen atoms were added theoretically and difference-Fourier map revealed the positions of the remaining atoms. All non-hydrogen atoms were refined anisotropically using a full-matrix least-squares procedure on F^2 with SHELXL-2014[52b]. The structure contained large void, and the solvent molecules and the positive or negative ions locating in the void couldn′t be identified because they were highly disordered and had so small residual peak. Therefore, SQUEEZE in PLATON program was performed to remove the highly disordered solvent and ions. The structures were then refined again using the data generated. The crystal data and experimental parameters relevant to the structure determinations are listed in Table 1.

CCDC: 1589650, **1**; 1589813, **2**.

Table 1　Crystal data and structure refinement parameters for complexes 1 and 2

Complex	1	2
Formula	$C_{50}H_{70}Ni_3N_4O_{18}$	$C_{52}H_{70}Ni_3N_8O_{24}$
Formula weight	1 191.23	1 367.29
Crystal system	Trigonal	Triclinic
Space group	$R\bar{3}$	$P\bar{1}$
a / nm	3.651 4(2)	0.980 80(10)
b / nm	3.651 4(2)	1.088 56(12)
c / nm	1.213 53(7)	1.564 37(9)
α / (°)		97.265(6)
β / (°)		90.468(6)
γ / (°)		95.428(9)

Continued Table 1

V / nm^3	14.012(2)	1.649 0(3)
Z	9	1
D_c / (g·cm^{-3})	1.271	1.377
μ / mm^{-1}	0.963	0.927
F(000)	5 634	714
Crystal size / mm	0.33×0.31×0.27	0.11×0.13×0.21
θ range / (°)	3.597~26.022	3.344~26.022
Index ranges	$-45 \leqslant h \leqslant 29, -45 \leqslant k \leqslant 44, -14 \leqslant l \leqslant 14$	$-12 \leqslant h \leqslant 12, -13 \leqslant k \leqslant 11, -19 \leqslant l \leqslant 17$
Reflection collected	13 730	10 927
Independent reflection	5 942	6 409
R_{int}	0.042 6	0.063
Completeness / %	97.3	98.8
Data, restraint, parameter	5 942, 105, 355	6 409, 72, 417
GOF	1.043	1.031
Final R_1, wR_2 [$I>2\sigma(I)$]	0.079 1, 0.223 9	0.083 7, 0.194 9
R_1, wR_2 indices (all data)	0.121 6, 0.261 9	0.152 4, 0.255 8

[a] $R_1=\sum||F_o|-|F_c||/\sum|F_o|$; [b] $wR_2=\{\sum w(F_o^2-F_c^2)^2/\sum[w(F_o^2)]^2\}^{1/2}$.

2 Results and discussion

2.1 IR spectra

The FT-IR spectra of H_2L^1 and H_2L^2 with their corresponding complexes **1** and **2** exhibited various bands in the 4 000~400 cm^{-1} region (Fig.1 and Table 2). The infrared spectra of the ligand H_2L^1 and its complex **1** are shown in Fig.1(a). The ligand H_2L^1 had a strong absorption peak at 3 165 cm^{-1}, which belongs to the stretching vibration of the phenolic hydroxyl groups, while complex **1** exhibited a new vibration peak at 3 405 cm^{-1}, indicating the presence of n-butanol molecules. This result is consistent with the previous element analysis results. It can be seen from Fig.1 and Table 2 that the stretching vibration absorption peak of the $\nu_{C=N}$ bond in the ligand H_2L^2

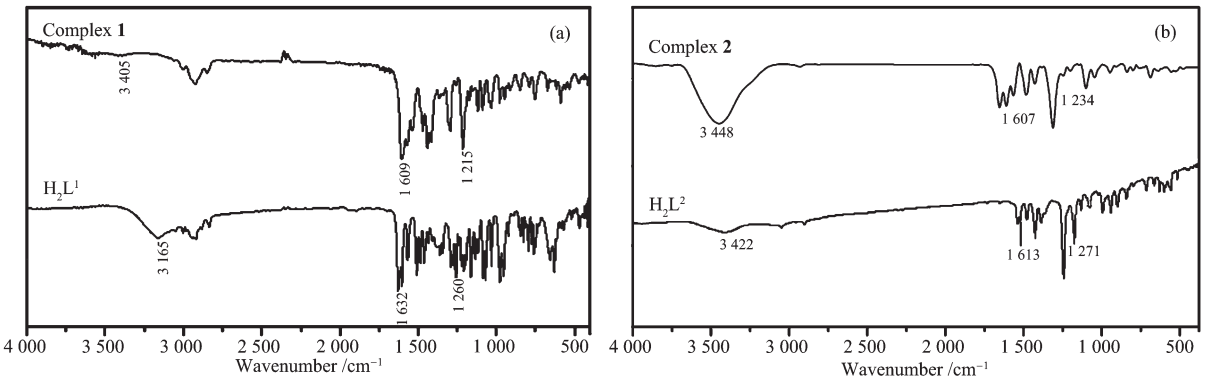

Fig.1 FT-IR spectra of the ligands and their complexes **1** and **2**

Table 2 Main absorption peaks in FT-IR spectra of the ligands and their complexes 1 and 2

cm^{-1}

Compound	ν_{O-H}	$\nu_{C=N}$	ν_{Ar-O}	ν_{Ni-N}	ν_{Ni-O}
H_2L^1	3 165	1 632	1 260	—	—
Complex **1**	3 405	1 609	1 215	590	419
H_2L^2	3 422	1 613	1 271	—	—
Complex **2**	3 448	1 607	1 234	552	422

appeared at 1 632 cm^{-1}, and that of complex **1** appeared at 1 609 cm^{-1}. The peak-to-low wavenumber is shifted by 23 cm^{-1} [64-65], indicating that the Ni(Ⅱ) ions coordinate to the oxime nitrogen atoms, giving rise to reduction in the bond energy of the C=N bond.

As shown in Fig.1(b), the stretching vibration absorption peaks of $\nu_{C=N}$ and ν_{Ar-O} in the ligand H_2L^2 appeared near 1 613 and 1 271 cm^{-1}, whereas those of complex **2** appeared at 1 607 and 1 234 cm^{-1}, respectively[66-67], and moving toward the direction of low wave number.

The far-IR spectra (550 ~100 cm^{-1}) of both complexes **1** and **2** were also obtained so as to identify the bonds of Ni-O and Ni-N frequencies. The bands at 419 and 422 cm^{-1} of complexes **1** and **2** can be attributed to ν_{Ni-O}, while the bands at 590 and 552 cm^{-1} are assigned to ν_{Ni-N}, respectively[34].

2.2 UV-Vis spectra

The UV-Vis absorption spectra of the free ligands H_2L^1 and H_2L^2 with their corresponding complexes **1** and **2** in ethanol solutions (10 μmol·L^{-1}) at 298 K are shown in Fig.2.

Obviously, the absorption peaks of the ligands H_2L^1 and H_2L^2 differ from those of complexes **1** and **2**. From Fig.2(a), we can see that the ligand H_2L^1 showed two strong absorption peaks appear near 274 and 309 nm. The former belongs to the π-π* transition of the benzene rings in the ligand molecule. The latter is assigned to the transition absorption peak of n-π* on the C=N bonds[68-69]. Compared with the π-π* transition absorption peak of the benzene rings at 274 nm of the ligand H_2L^1, it was red-shifted to 279.5 nm in complex **1**, indicating that the Ni(Ⅱ) ions have coordinated to the ligand H_2L^1. At the same time, the absorption peak of the ligand H_2L^1 appearing near 309 nm disappeared in complex **1**, indicating that the oxime nitrogen atoms have coordinated with the Ni(Ⅱ) ions. In addition, complex **1** exhibited a new absorption peak at 349 nm. It can be seen that the Ni(Ⅱ) ions chelate with two oxime nitrogen atoms and two phenol oxygen atoms to produce a charge transfer effect.

As shown in Fig.2(b), the ligand H_2L^2 showed two absorption peaks appearing around 375 and 448 nm. The absorption peak near 375 nm is attributed to the π-π* transition of the aromatic rings in the ligand H_2L^2, and the absorption peak at 448 nm is attributed to the π-π* transition of the C=N bonds in H_2L^2. However, compared with the ligand H_2L^2, the positions of the absorption peaks of complex **2** were blue-shifted, and the absorption peak at 448 nm was blue-shifted by about 51 nm, while the absorption peak of the ligand H_2L^2 near 375 nm disappeared. It is indicated that there are strong coordination bonds between the ligand H_2L^2 and the Ni(Ⅱ) ions in complex **2**.

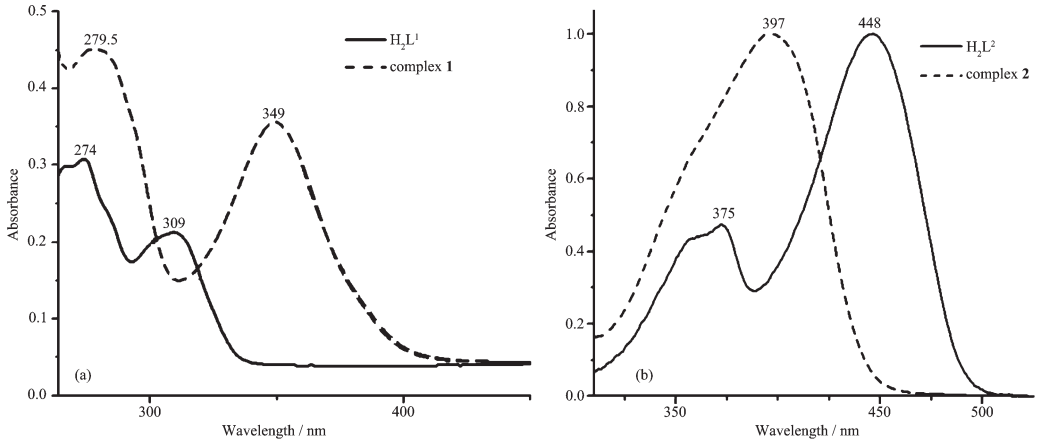

Fig.2　UV-Vis spectra of the ligands and their complexes **1** and **2**

2.3 Descriptions of crystal structures

2.3.1 Crystal structure of complex **1**

As shown in Fig.3, in the crystal structure of complex **1**, the terminal hexa-coordinated Ni(Ⅱ) ion (Ni1) is located in the *cis*-N_2O_2 coordination cavity (O1, O4, N1 and N2) of the completely deprotonated

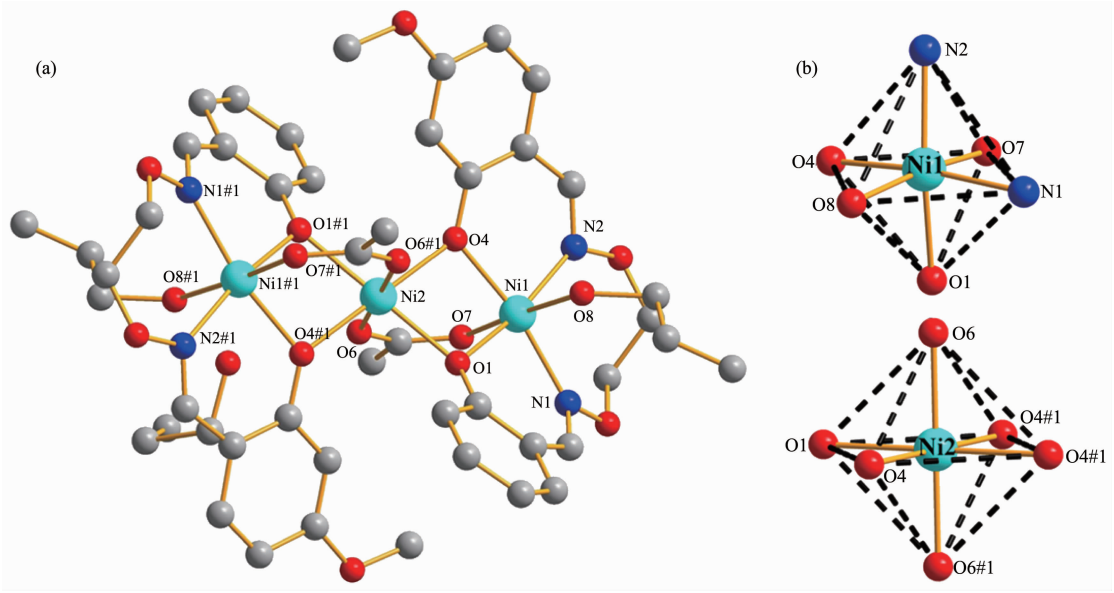

Hydrogen atoms and solvent molecules are omitted for clarity; Symmetry codes: #1: 1−*x*, −*y*, 1−*z*

Fig.3 (a) Molecular structure and atom numberings of complex **1** with 30% probability displacement ellipsoids; (b) Coordination polyhedrons for Ni(Ⅱ) ions of complex **1**

Table 3 Selected bond lengths (nm) and angles (°) for complex 1

Ni1-O1	0.201 1(5)	Ni1-N1	0.206 9(5)	Ni2-O1	0.208 2(4)
Ni1-O4	0.201 7(4)	Ni1-N2	0.205 1(7)	Ni2-O4	0.206 0(5)
Ni1-O8	0.216 2(5)	Ni1-O7	0.203 5(4)	Ni2-O6	0.209 5(4)
O7#1-Ni1-N2	92.7(2)	O4-Ni1-N2	88.5(2)	O1-Ni2-O6	92.11(15)
O1-Ni1-O4	81.17(18)	O4-Ni1-O7#1	90.27(18)	O1-Ni2-O1#1	180.00
O1-Ni1-O8	88.1(2)	O8-Ni1-N1	87.3(2)	O1-Ni2-O4#1	101.54(17)
O1-Ni1-N1	86.2(2)	O8-Ni1-N2	86.6(2)	O1-Ni2-O6#1	87.89(15)
O1-Ni1-N2	168.11(18)	O7#1-Ni1-O8	176.45(19)	O4-Ni2-O6	89.59(18)
O1-Ni1-O7#1	93.3(2)	O7#1-Ni1-N1	89.5(2)	O4-Ni2-O4#1	180.00
O4-Ni1-O8	93.19(18)	N1-Ni1-N2	104.1(2)	O4-Ni2-O6#1	90.41(18)
O4-Ni1-N1	167.4(2)	O1-Ni2-O4	78.47(17)	O6-Ni2-O6#1	180.00

Symmetry codes: #1: 1−*x*, −*y*, 1−*z*.

$(L^1)^{2-}$ unit, and one μ-acetate oxygen atom (O7) and one coordinated *n*-propanol oxygen atom (O8) occupy together the axial positions. Meanwhile, the coordination environment of the central hexa-coordinated Ni(Ⅱ) ion (Ni2) is completed by quadruple μ-phenoxo oxygen atoms from the two $(L^1)^{2-}$ moieties and two μ-acetate oxygen atoms (O6 and O6#1). All of the six oxygen atoms coordinate to Ni2 constituting an octahedral geometry. The μ-acetate ligand serves as bridging group for Ni1 and Ni2 and another coordinates to Ni2 and Ni1#1, in both cases via Ni-O-C-O-Ni bridges. Then, all of the hexa-coordinated Ni(Ⅱ) ions of complex **1** have slightly distorted octahedral geometries[23].

In the crystal structure of complex **1**, there are two pairs of intra-molecular hydrogen bonding interactions (C8−H8B⋯O7#2 and C13−H13⋯O1#2) (Fig.4) [53-57]. Table 4 summarizes the intra-molecular hydrogen bonding interactions in complex **1**. As shown in Fig.5 and Table 4, the supramolecular structure of complex **1** was linked by inter-molecular hydrogen bonding interactions (O8−H8⋯O9, O9−H9⋯O6 and C8−H8A⋯O5#1), which performs a crucial role in constructing and stabilizing 1D supramolecular chain structure[58].

Table 4　Hydrogen bonding interactions for complex 1

D–H···A	*d*(D-H) / nm	*d*(H···A) / nm	*d*(D···A) / nm	∠D–H···A / (°)
O8–H8···O9	0.086(6)	0.177(6)	0.262 7(10)	172(12)
O9–H9···O6	0.082	0.206	0.277 9(9)	146
C8–H8A···O5#1	0.097	0.253	0.317 7(9)	124
C8–H8B···O7#2	0.097	0.229	0.314 3(11)	146
C13–H13···O1#2	0.093	0.256	0.327 7(8)	134

Symmetry codes: #1: *x*, *y*, 1+*z*; #2: 1–*x*, –*y*, 1–*z*.

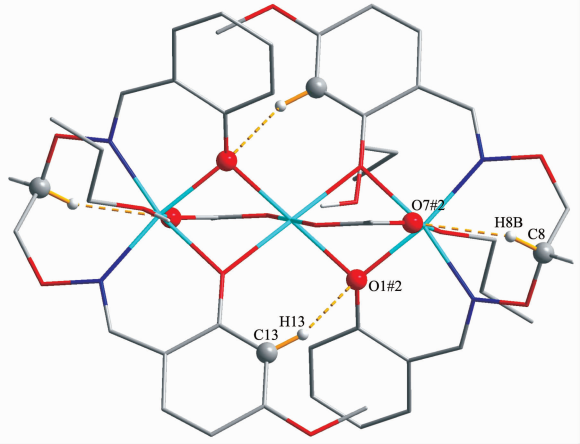

Hydrogen atoms are omitted except those forming hydrogen bonds; Symmetry codes: #2: 1–*x*, –*y*, 1–*z*

Fig.4　View of the intra-molecular hydrogen bonding interaction of complex **1**

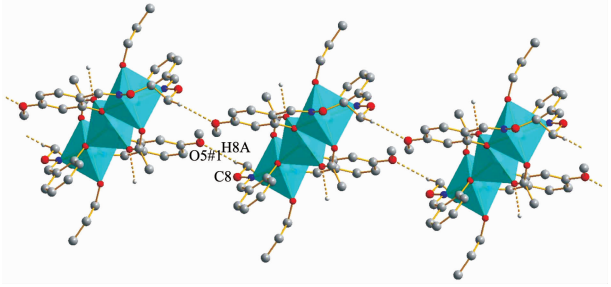

Symmetry codes: #1: *x*, *y*, 1+*z*

Fig.5　View of inter-molecular hydrogen bonding interactions of complex **1**

2.3.2 Crystal structure of complex **2**

X-ray crystallographic analysis of complex **2** revealed symmetric trinuclear structure. It crystallizes in the triclinic system, space group $P\bar{1}$. Three Ni(Ⅱ) ions, two completely deprotonated $(L^{2})^{2-}$ units, two coordinated *n*-butanol molecules and two μ-acetate result in a symmetrical trinuclear Ni(Ⅱ) complex. Selected bond lengths and angles are listed in Table 5.

As shown in Fig.6, the hexa-coordinated terminal Ni(Ⅱ) ion (Ni1 or Ni#1) lies in the N_2O_2 coordination sphere (O1, O8, N2 and N3 or O1#1, O8#1, N2#1 and N3#1) of $(L^{2})^{2-}$, and coordinates with one μ-acetate oxygen atom (O9 or O9#1) and one coordinated *n*-butanol oxygen atom (O11 or O11#1).

As illustrated in Fig.7, in the crystal structure of complex **2**, there are six pairs of intra-molecular hydrogen bonding interactions (C0AA –H0AA ··· O3,

Table 5　Selected bond lengths (nm) and angles (°) for complex 2

Ni1-O1	0.202 7(5)	Ni1-O11	0.210 0(6)	Ni2-O1	0.208 0(4)
Ni1-O8	0.202 9(4)	Ni1-N3	0.207 9(6)	Ni2-O8	0.206 8(5)
Ni1-O9	0.203 3(5)	Ni1-N2	0.208 7(6)	Ni2-O10	0.201 1(5)
O1-Ni1-O8	80.67(18)	O8-Ni1-N3	85.9(2)	O8-Ni2-O10	87.92(19)
O1-Ni1-O9	89.40(19)	O9-Ni1-O11	176.9(2)	O8-Ni2-O8#1	180.00
O1-Ni1-O11	92.4(2)	O9-Ni1-N2	90.0(2)	O8-Ni2-O10#1	92.08(19)
O1-Ni1-N2	87.7(2)	O9-Ni1-N3	91.4(2)	O1#1-Ni2-O8#1	78.53(18)
O1-Ni1-N3	166.6(2)	O1-Ni2-O10	89.98(18)	O11-Ni1-N2	87.6(2)
O8-Ni1-O9	94.4(2)	O1-Ni2-O1#1	180.00	O11-Ni1-N3	87.4(2)
O8-Ni1-O11	88.4(2)	O1-Ni2-O8#1	101.48(18)	N2-Ni1-N3	105.7(2)
O8-Ni1-N2	167.5(2)	O1-Ni2-O10#1	90.02(18)	O1-Ni2-O8	78.53(18)

Symmetry codes: #1: 2–*x*, 1–*y*, 2–*z*.

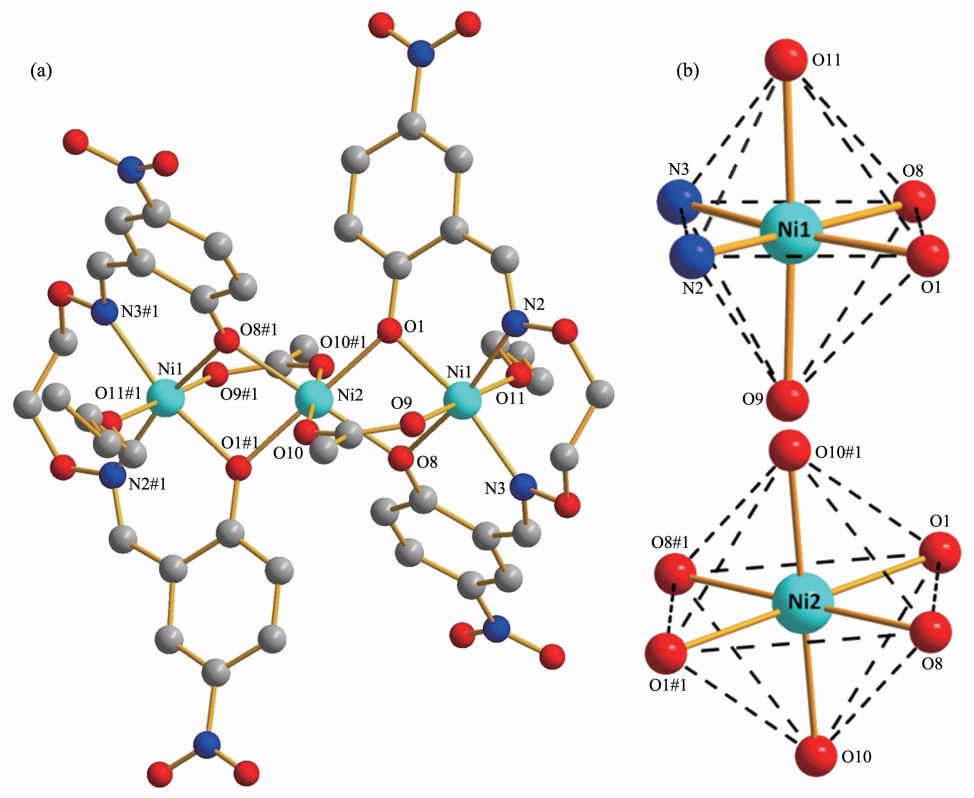

Solvent molecules and hydrogen atoms are omitted for clarity; Symmetry codes: #1: 2–*x*, 1–*y*, 2–*z*

Fig.6 (a) Molecular structure and atom numberings of complex **2** with 30% probability displacement ellipsoids; (b) Coordination polyhedrons for Ni(Ⅱ) ions of complex **2**

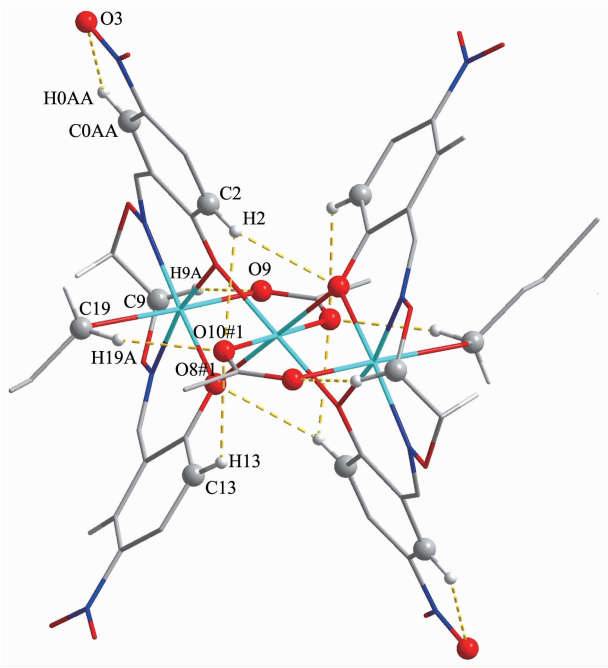

Hydrogen atoms, except those forming hydrogen bonds, are omitted for clarity; Symmetry codes: #1: 2–*x*, 1–*y*, 2–*z*

Fig.7 Intra-molecular C–H···O hydrogen bonding interactions of complex **2**

C2–H2···O8#1, C2–H2···O10#1, C9–H9A···O9, C13–H13···O10#1 and C19–H19A···O10#1)[59-63]. As shown in Fig.8 and Table 6, complex **2** molecules are linked into an infinite 2D supramolecular structure by inter-molecular hydrogen bonding interactions (C19–H19B···O3#2, C23–H23B···O7#3).

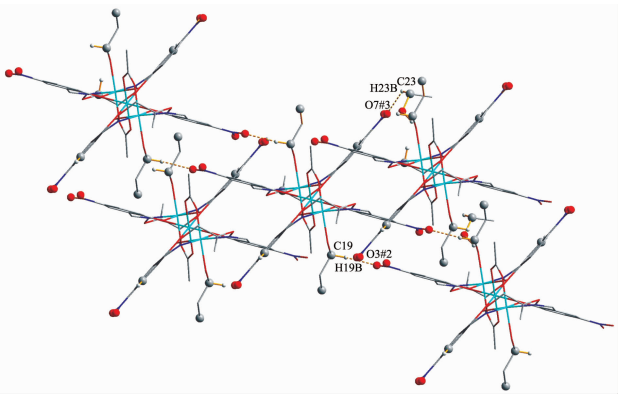

Symmetry codes: #2: 1–*x*, –*y*, 2–*z*; #3: *x*, –1+*y*, *z*

Fig.8 Two dimensional supramolecular structure formed by inter-molecular C–H···O hydrogen bonding interactions in complex **2**

Table 6　Hydrogen bonding interactions for complex 2

D–H···A	*d*(D-H) / nm	*d*(H···A) / nm	*d*(D···A) / nm	∠D–H···A / (°)
C0AA–H0AA···O3	0.093	0.237	0.269 0(11)	100
C2–H2···O8#1	0.093	0.257	0.329 2(9)	135
C2–H2···O10#1	0.093	0.257	0.216 5(9)	122
C9–H9A···O9	0.097	0.221	0.309 5(12)	150
C13–H13···O10#1	0.093	0.254	0.313 5(8)	122
C19–H19A···O10#1	0.097	0.248	0.343 2(11)	167
C19–H19B···3#2	0.097	0.252	0.330 1(12)	137
C23–H23B···O7#3	0.097	0.246	0.320(2)	133

Symmetry codes: #1: 2–*x*, 1–*y*, 2–*z*; #2: 1–*x*, –*y*, 2–*z*; #3: *x*, –1+*y*, *z*.

2.4　Hirshfeld surfaces analyses

The Hirshfeld surfaces[70] of complexes **1** and **2** are illustrated in Fig.9 showing surfaces that have been mapped over d_{norm} and the corresponding location in shape index exists the complementary region of red concave surface surrounded by receptors and the blue convex surface surrounding receptors, further proving that such hydrogen bonding exists. As for the large amount of white region in d_{norm} surfaces, it is suggested that there is a weaker and farther contact between molecules, rather than hydrogen bonding.

Fig.10 shows the 2D plots generated[71] from the Hirshfeld surfaces of complexes **1** and **2** corresponding to the O···H, C···H and H···H interactions. As shown in Fig.10(a), the H···H interactions appeared at (0.115 nm, 0.115 nm) accounting for 66.6% of the total area of Hirshfeld surfaces for complex **1**. The C···H/H···C interactions in a range of (0.160 nm, 0.09 nm) appeared as a pair of symmetrical wings, accounting for 11.6% of the total area of Hirshfeld surfaces. The proportions of O···H/H···O interactions comprised 14.2% of the total Hirshfeld surfaces for each molecule of complex **1**. As shown in Fig.10(b), for complex **2**, the interactions of H···H appeared at (0.115 nm, 0.115nm) accounting for 44.8% of the total area of Hirshfeld surfaces. The C···H/H···C interactions in a range of (0.160 nm, 0.105 nm) accounted for 10.1% of the total area of Hirshfeld surfaces. The proportions of O···H/H···O interactions comprised 37% of the total Hirshfeld surfaces for each molecule of complex **2**. It is because of the existence of these weaker hydrogen bonds that complexes **1** and **2** can be stable.

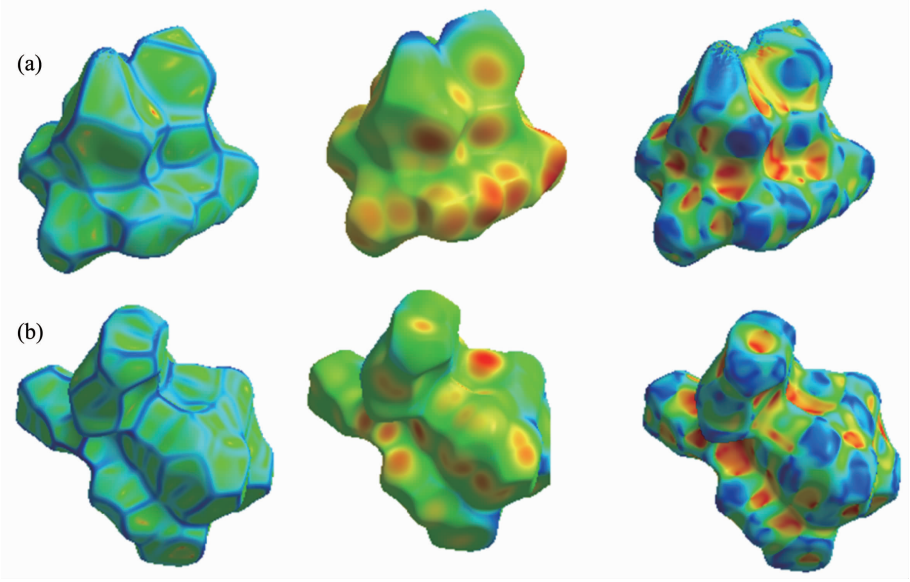

Fig.9　Hirshfeld surfaces analyses mapped with curvedness, d_{norm} and shape index of complexes **1** and **2**

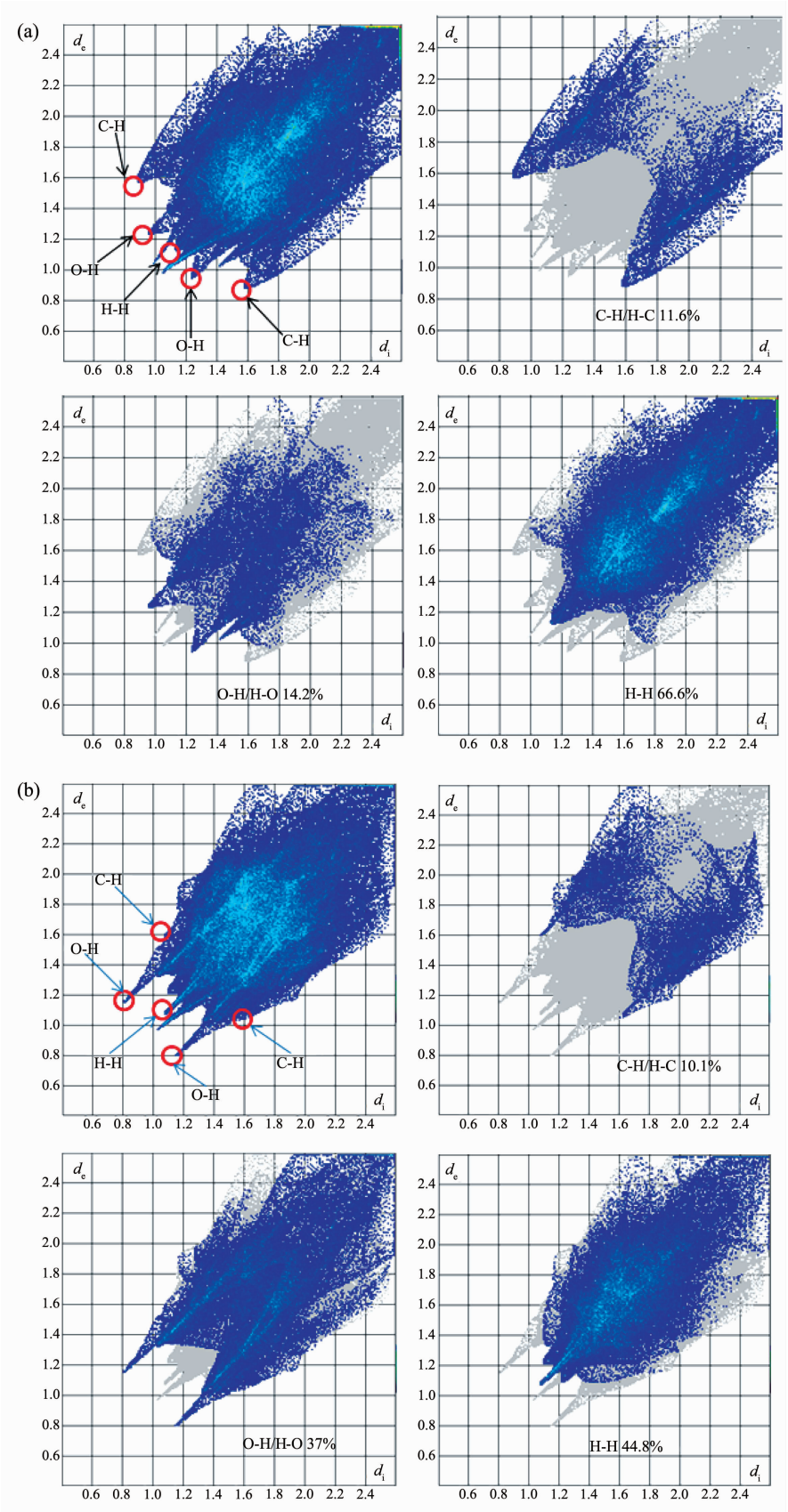

Fig.10 Fingerprint plots of complexes **1** and **2**: full and resolved into O···H, C···H and H···H contacts showing the percentages of contacts contributed to the total Hirshfeld surface area of molecule

3 Conclusions

In summary, we have reported the successful syntheses and characterizations of two newly designed trinuclear Ni(Ⅱ) Salamo-type complexes, {[Ni(L^1)(*n*-propanol)]$_2$(OAc)$_2$Ni}·2(*n*-propanol) (**1**) and {[Ni(L^2)(*n*-butanol)]$_2$(OAc)$_2$Ni}·2(*n*-butanol) (**2**). All of the hexa-coordinated Ni(Ⅱ) ions in complexes **1** and **2** are slightly distorted octahedral configurations, and complex **1** forms an infinite 1D chain-like supramolecular structure through inter-molecular hydrogen bonding interactions. The supramolecular structure of complex **2** is formed by inter-molecular hydrogen bonding interactions, resulting in a self-assembled infinite 2D supramolecular network.

Acknowledgements: This work was supported by the National Natural Science Foundation of China (Grant No. 21761018) and the Program for Excellent Team of Scientific Research in Lanzhou Jiaotong University (Grant No.201706), which are gratefully acknowledged.

References:

[1] Chai L Q, Tang L J, Chen L C, et al. *Polyhedron*, **2017**,**122**: 228-240

[2] Wu H L, Wang C P, Wang F, et al. *J. Chin. Chem. Soc.*, **2015**,**62**:1028-1034

[3] Song X Q, Liu P P, Xiao Z R, et al. *Inorg. Chim. Acta*, **2015**, **438**:232-244

[4] Sun Y X, Wang L, Dong X Y, et al. *Synth. React. Inorg. Met.-Org. Nano-Met. Chem.*, **2013**,**43**:599-603

[5] Chai L Q, Mao K H, Zhang J Y, et al. *Inorg. Chim. Acta*, **2017**,**457**:34-40

[6] Zhao L, Wang L, Sun Y X, et al. *Synth. React. Inorg. Met.-Org. Nano-Met. Chem.*, **2012**,**42**:1303-1308

[7] Wang P, Zhao L. *Synth. React. Inorg. Met-Org. Nano-Met. Chem.*, **2016**,**46**:1095-1101

[8] Zhao L, Dang X T, Chen Q, et al. *Synth. React. Inorg. Met.-Org. Nano-Met. Chem.*, **2013**,**43**:1-6

[9] Dong X Y, Kang Q P, Li X Y, et al. *Crystals*, **2018**,**8**:139

[10]Wu H L, Pan G L, Bai Y C, et al. *Res. Chem. Intermed.*, **2015**,**41**:3375-3388

[11]Wu H L, Pan G L, Bai Y C, et al. *J. Coord. Chem.*, **2013**, **66**:2634-2646

[12]Wu H L, Pan G L, Bai Y C, et al. *J. Chem. Res.*, **2014**,**38**: 211-217

[13]Wang F, Xu Y L, Aderinto S O, et al. *J. Photochem. Photobiol. A*, **2017**,**332**:273-282

[14]Chen C Y, Zhang J W, Zhang Y H, et al. *J. Coord. Chem.*, **2015**,**68**:1054-1071

[15]Li X Y, Kang Q P, Liu L Z, et al. *Crystals*, **2018**,**8**:43

[16]Wu H L, Pan G L, Wang H, et al. *J. Photochem. Photobiol. B*, **2014**,**135**:33-43

[17]Sun S S, Stern C L, Nguyen S T, et al. *J. Am. Chem. Soc.*, **2004**,**126**:6314-6326

[18]Ren Z L, Hao J, Hao P, et al. *Z. Naturforsch.*, **2018**,**73**:203-210

[19]Song X Q, Cheng G Q, Liu Y A, et al. *Inorg. Chim. Acta*, **2016**,**450**:386-394

[20]Dong X Y, Akogun S F, Zhou W M, et al. *J. Chin. Chem. Soc.*, **2017**,**64**:412-419

[21]Song X Q, Peng Y J, Chen G Q, et al. *Inorg. Chim. Acta*, **2015**,**427**:13-21

[22]Zhang L W, Li X Y, Kang Q P. *Crystals*, **2018**,**8**:173

[23]Kang Q P, Li X Y, Zhao Q, et al. *Appl. Organomet. Chem.*, **2018**,**32**:e4379

[24]Dong W K, Zhang J, Zhang Y, et al. *Inorg. Chim. Acta*, **2016**,**444**:95-102

[25]Wang L, Ma J C, Dong W K, et al. *Z. Anorg. Allg. Chem.*, **2016**,**642**:834-839

[26]Dong W K, Zhu L C, Dong Y J, et al. *Polyhedron*, **2016**, **117**:148-154

[27]Li J, Zhang H J, Chang J, et al. *Crystals*, **2018**,**8**:176

[28]Dong W K, Ma J C, Dong Y J, et al. *Polyhedron*, **2016**,**115**: 228-235

[29]Dong W K, Ma J C, Zhu L C, et al. *New J. Chem.*, **2016**,**40**: 6998-7010

[30]Song X Q, Liu P P, Liu Y A, et al. *Dalton Trans.*, **2016**,**45**: 8154-8163

[31]Liu Y A, Wang C Y, Zhang M, et al. *Polyhedron*, **2017**,**127**: 278-286

[32]Ömer S, Ümmühan Ö Ö, Nurgul S, et al. *Tetrahedron*, **2016**, **72**:5843-5852

[33]Chai L Q, Zhou L, Zhang K Y, et al. *Appl. Organomet. Chem.*, **2018**:e4576

[34]Dong W K, Ma J C, Zhu L C, et al. *Inorg. Chim. Acta*, **2016**, **445**:140-148

[35]Dong X Y, Li X Y, Liu L Z, et al. *RSC Adv.*, **2017**,**7**:48394-48403

[36]Chen L, Dong W K, Zhang H, et al. *Cryst. Growth Des.*, **2017**,**17**:3636-3648

[37]Chai L Q, Wang G, Sun Y X, et al. *J. Coord. Chem.*, **2012**, **65**:1621-1631

[38]Zhou L, Hu Q, Chai L Q, et al. *Polyhedron*, **2019**,**158**:102-116

[39]Akine S, Taniguchi T, Dong W K, et al. *J. Org. Chem.*, **2005**,**70**:1704-1711

[40]Peng Y D, Li X Y, Kang Q P, et al. *Crystals*, **2018**,**8**:107

[41]Wang F, Liu L Z, Gao L, et al. *Spectrochim. Acta Part A*, **2018**,**203**:56-64

[42]Peng Y D, Wang F, Gao L, et al. *J. Chin. Chem. Soc.*, **2018**, **65**:893-899

[43]Dong W K, Lan P F, Zhou W M, et al. *J. Coord. Chem.*, **2016**,**69**:1-22

[44]Zhang L W, Liu L Z, Wang F, et al. *Molecules*, **2018**,**23**:1141

[45]Dong X Y, Zhao Q, Kang Q P, et al. *Crystals*, **2018**,**8**:230

[46]Wang F, Gao L, Zhao Q, et al. *Spectrochim. Acta Part A*, **2018**,**190**:111-115

[47]WANG Li(王莉), KANG Quan-Peng(康全鹏), HAO Jing(郝静), et al. *Chinese J. Inorg. Chem.*(无机化学学报), **2018**, **34**:525-533

[48]Dong X Y, Zhao Q, Wei Z L, et al. *Molecules*, **2018**,**23**: 1006

[49]Gao L, Liu C, Wang F, et al. *Crystals*, **2018**,**8**:77

[50]Hao J, Li X Y, Zhang Y, et al. *Materials*, **2018**,**11**:523

[51]Jia H R, Li J, Sun Y X, et al. *Crystals*, **2017**,**7**:247

[52](a)Sheldrick G M. *SADABS*, University of Göttingen, Germany, **1996**.

(b)Sheldrick G M. *Acta Crystallogr., Sect. C*: *Cryst. Struct. Commun.*, **2015**,**C71**:3-8

[53]Dong W K, Zheng S S, Zhang J T, et al. *Spectrochim. Acta Part A*, **2017**,**184**:141-150

[54]Chai L Q, Huang J J, Zhang H S, et al. *Spectrochim. Acta Part A*, **2014**,**131**:526-533

[55]SUN Yin-Xia(孙银霞), ZHAO Ya-Yuan(赵亚元), LI Chun-Yu(李春宇), et al. *Chinese J. Inorg. Chem.*(无机化学学报), **2016**,**32**:913-920

[56]Chai L Q, Liu G, Zhang J Y, et al. *J. Coord. Chem.*, **2013**, **66**:3926-3938

[57]Chai L Q, Zhang K Y, Tang L J, et al. *Polyhedron*, **2017**, **130**:100-107

[58]Guo W T, Li X Y, Kang Q P, et al. *Crystals*, **2018**,**8**:154

[59]Dong W K, Zhang X Y, Sun Y X, et al. *Synth. React. Inorg. Met.-Org. Nano-Met. Chem.*, **2015**,**45**:956-962

[60]Sun Y X, Xu L, Zhao T H, et al. *Synth. React. Inorg. Met.-Org. Nano-Met. Chem.*, **2013**,**43**:509-513

[61]ZHANG Hong-Jia(张宏佳), CHANG Jian(常健), JIA Hao-Ran(贾浩然), et al. *Chinese J. Inorg. Chem.*(无机化学学报), **2018**,**34**(12):2261-2270

[62]CHANG Jian(常健), ZHANG Hong-Jia(张宏佳), JIA Hao-Ran(贾浩然), et al. *Chinese J. Inorg. Chem.*(无机化学学报), **2018**,**34**(11):2097-2107

[63]Chai L Q, Huang J J, Zhang J Y, et al. *J. Coord. Chem.*, **2015**,**68**:1224-1237

[64]Zhang H, Dong W K, Zhang Y, et al. *Polyhedron*, **2017**,**133**: 279-293

[65]YANG Yu-Hua(杨玉华), HAO Jing(郝静), DONG Yin-Juan(董银娟), et al. *Chinese J. Inorg. Chem.*(无机化学学报), **2017**,**33**:1280-1292

[66]Zhao L, Dang X T, Chen Q, et al. *Synth. React. Inorg. Met.-Org. Nano-Met. Chem.*, **2013**,**43**:1241-1246

[67]Dong X Y, Gao L, Wang F, et al. *Crystals*, **2017**,**7**:267

[68]Sun Y X, Gao X H. *Synth. React. Inorg. Met.-Org. Nano-Met. Chem.*, **2011**,**41**:973-978

[69]Li G, Hao J, Liu L Z, et al. *Crystals*, **2017**,**7**:217

[70]Rohl A L, Moret M, Kaminsky W, et al. *Cryst. Growth Des.*, **2012**,**8**:4517-4525

[71]Chattopadhyay B, Mukherjee A K, Narendra N, et al. *Cryst. Growth Des*., **2010**,**10**:65-68